Influence of the Drum Position Parameters and the Ranging Arm Thickness on the Coal Loading Performance

Kuidong Gao [1,2,*], Changlong Du [2], Jianghui Dong [3,*] and Qingliang Zeng [4]

[1] College of Mechanical & Electrical Engineering, Shandong University of Science & Technology, Qingdao 266590, China
[2] School of Mechanical & Electrical Engineering, China University of Mining & Technology, Xuzhou 221116, China; jdjxx3@cumt.edu.cn
[3] School of Natural and Built Environments, University of South Australia, Adelaide, SA 5095, Australia
[4] College of Mechanical & Electrical Engineering, Shandong University of Science & Technology, Qingdao 266590, China; qlzeng@sdust.edu.cn
* Correspondence: gaokuidong@cumt.edu.cn (K.G.); Jianghui.dong@unisa.edu.au (J.D.); Tel./Fax: +86-532-8605-7559 (K.G.); +61-088-357-9928 (J.D.)

Abstract: The poor coal loading performance of a shearer drum primarily restricts the widespread application of the shearer and affects the mining efficiency in thin seam mining. The coal loading performance of the shearer drum is influenced by several factors, such as geographical environment, drum structural parameters, and motion parameters. In addition to the above factors, in the actual production, the coal loading performance of the shearer drum is also affected significantly by the drum position parameters and the structural parameters of the connected equipment, e.g., the thickness of the ranging arm. The influence of the parameters on the coal loading performance of the shearer drum was studied using a three-dimensional (3D) discrete element method (DEM) simulation in the current study, and the trends of the influential parameters were obtained. Therefore, the results of this study can provide technical guidance for thin seam shearer structural design, associated equipment selection, and mining technology selection, thus improving the mining efficiency and reducing the labor cost.

Keywords: shearer drum; coal mining; discrete element method; coal loading performance; shearer structure; ranging arm

1. Introduction

A thin seam refers to the coal seam thickness, which is less than 1.7 m in Europe and America. However, in China, the thickness of the thin seam is less than 1.3 m. A thin seam shearer is used for mining thin seams in China. Additionally, a medium seam shearer or a thick seam shearer is used for a coal seam thicker than 1.3 m. In China, due to the different definitions of the seam height, the working height of the thin seam shearer is lower, and the drum diameter is smaller. Furthermore, the roller blade space capacity of the seam is extremely small, and the seam shearer capacity through the space is even smaller. Due to the influence of the above-mentioned two aspects, the loading rate of the shearer drum is extremely low for the thin seam shearer in China, typically under 70%. The coal is not loaded to the scraper conveyor and becomes float coal, which is left on the shearer track. The float coal has to be manually cleaned, which increases the work load and cost. Therefore, the low coal loading rate of the shearer drum has affected the general use of the shearer in thin seam mining and the improvement in mining efficiency.

Studies on the coal loading performance of the shearer drum are relatively rare, and most of them were performed earlier. In the 1980s and 1990s, the key factors affecting the coal loading performance of the shearer drum were discussed and studied. The effects of mining conditions, structural parameters, and working parameters of the shearer and mining technology on the loading rate of the shearer drum were presented in their studies using theoretical analysis, worksite statistical analysis, and computer technology. The studies had a positive role in guiding the shearer design using a mining wall with a height greater than 1.7 m [1–4]. Based on their experiences, American scholars Peng and Chiang proposed "Longwall Mining" [5]. Several primary factors, which influenced the coal loading performance of the shearer drum, were noted, and precautions were suggested. Furthermore, Turkish mentioned that the distance of the drum to the scraper conveyor could affect the coal loading performance of the shearer drum [6]. Additionally, it was indicated that the drum with a conical hub had a better coal loading performance than that of a cylindrical hub [7]. The coal loading performance of the shearer drum can be increased using a helical vane in the form of a varying pitch and a curved generatrix [8]. An experimental modeling method was used by Liu and Gao [9–11] to study the effects of the vane helix angle, rotation speed, and pulling speed on the coal loading rate.

It is difficult to directly use the research results to guide the design and usage of the thin seam shearer because most of the earlier studies focused on a medium or thick seam shearer. Although the effects of the scraper conveyor on the coal loading performance of the shearer drum were demonstrated in these studies, they were not described in detail [2,5,6]. Furthermore, the objective of their studies was also a medium or thick seam shearer, thus limiting the guidance for thin seam mining in China.

The discrete element method (DEM) is a computer simulation that has been widely used in several fields, e.g., geotechnical engineering, geology, and machinery fields [12–19], and especially the screw conveying field [20–23]. In the current study, we attempted to simulate the mining and loading processes using a thin seam shearer with PFC^{3D} (Ver.3.00) software. The primary objectives of this study were two-fold: (1) investigate the effects of the drum position parameters and the thickness of the ranging arm on the coal loading rate of the shearer drum using the DEM simulation; and (2) verify the feasibility and accuracy of the drum coal loading process simulation.

2. Mathematical Model [24]

Generally, PFC^{3D} (Itasca Consulting Group, Minneapolis, MN, USA) supports basic contact constitutive models, e.g., the contact-stiffness model, slip model, and bonding model. The contact-stiffness model is used to describe the relationship between the particle contact force and the displacement; the slip model is used to conduct the relative motion of each particle; and the bonding model is used to restrict the shear forces and the normal forces of the particles. In this study, the constitutive models of the particles were determined using the considered drum loading process and each model's serviceable range [25,26].

2.1. Contact-Stiffness Model

Essentially, there are two types of contact models in PFC^{3D}: a linear contact model and a Hertz-Mindlin contact model. Bonding cannot be used because tensile forces cannot be applied in the Hertz-Mindlin model. Therefore, the linear contact model has to be selected in this study; the adhesive force between the particles needs to be considered in the constitute coal seam, and the coal seams should have a certain shape before being mined.

The normal contact force and the shear contact force in the linear contact model can be described in Equation (1) as follows:

$$\begin{cases} F_i^n = K^n U^n n_i \\ \Delta F_i^s = -K^s \Delta U_i^s \end{cases} \tag{1}$$

where F_i^n is the normal contact force; ΔF_i^s is the shear contact force; K^n is the normal contact stiffness; K^S is the shear contact stiffness; U^n is the tangential displacement increment; n_i is the unit normal vector; ΔU_i^s is the shear component of the contact displacement-increment vector; and i is the number of particles.

The normal contact stiffness K^n can be expressed in Equation (2) as follows:

$$K^n = \frac{k_n^{[A]} k_n^{[B]}}{k_n^{[A]} + k_n^{[B]}} \tag{2}$$

where $k_n^{[A]}$ and $k_n^{[B]}$ are the normal stiffness of the contact particles.

The shear contact stiffness K^s can be expressed in Equation (3) as follows:

$$K^s = \frac{k_s^{[A]} k_s^{[B]}}{k_s^{[A]} + k_s^{[B]}} \tag{3}$$

where $k_s^{[A]}$ and $k_s^{[B]}$ are the normal stiffness of the contact particles.

2.2. Slip Model

The slip is enforced by verifying whether the maximum static friction force is exceeded by the shearing force. The maximum static friction force is calculated using the minimum friction coefficient μ, and this friction force can be expressed in Equation (4) as follows:

$$F^s{}_{\max} = \mu |F_i^n| \tag{4}$$

The slip will occur between the two contact elements, when the shear contact force F_i^s meets $|F_i^s| > F^s{}_{\max}$.

2.3. Bonding Model

Bonding models are used to determine the contact between two particles. PFC^{3D} provides two types of bonding models, *i.e.*, parallel bonding and contact bonding. Parallel bonding can transmit both force and moment while contact bonding can transmit force. Because the cutting force and the broken coal mode were not considered in this report, contact bonding can be used in the simulation. As indicated in Figure 1, the constitutive behavior for contact occurring at a point as well as the fatigue failure criterion of two bonding models can be expressed in Equation (5) as follows:

$$\begin{cases} F_n^c \geqslant R_n \,(\text{normal}) \\ F_s^c \geqslant R_s \,(\text{tangential}) \end{cases} \tag{5}$$

where R_n and R_s are the normal and the tangential bonding strength of the particles, respectively.
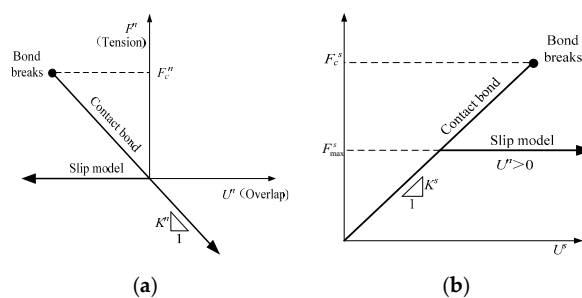
Figure 1. Constitutive behavior in the contact bonding model: (**a**) normal component of the contact force and (**b**) tangential component of the contact force.

3. Simulation Model Establishment

In the thin seam mining process, the thin seam shearer has to work with the associated support and conveyor equipment. The support equipment is used to protect the thin seam shearer by supporting the roof of the mined-out areas. The conveyor equipment is used to ensure continuous mining by loading the fallen coal. A thin seam shearer in operation is depicted in Figure 2. In an ideal mining condition, all of the fallen coals are conveyed onto the scrapers. However, some of the fallen coals are thrown into the mined-out area or the bottom of the drum due to the effect of the helical vanes. Additionally, because of the ranging arm, parts of the fallen coal loaded at the bottom of the drum are bounced back and become float coal or circling coal, whereas the other parts that are not bounced back are ejected. Because there is a considerable distance between the coal wall and the middle groove of the scraper conveyor, a few of the coals are loaded in this area and become float coal on the shearer track. Thus, it appears that the drum position parameters and the associated equipment's structural parameters have a significant effect on the coal loading rate.
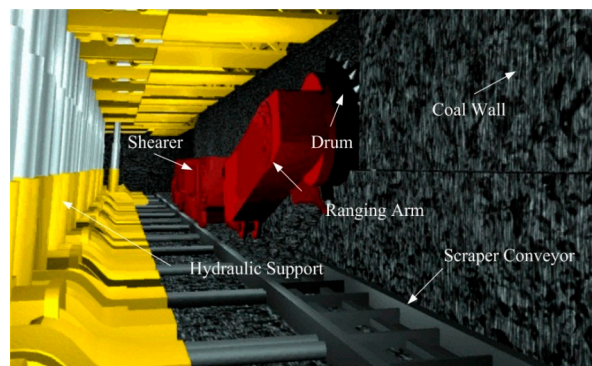

Figure 2. Shearer in operation.

The drum position is illustrated in Figure 3, where D_c is the drum diameter; G represents the distance between the bottom of the drum and the ranging arm; S represents the distance from the lowest section of the drum to the middle groove of the scraper conveyor; B is the thickness of the ranging arm; I is distance from the drum bottom to the floor; and L is the distance between the cell wall and the middle groove of the scraper conveyor. Because D_c is the drum's own parameter, I can be reduced by S, and the height of the middle groove of the scraper conveyor (L) is determined once the scraper conveyor is selected; thus, the effects of parameters B, S and L on the conveying performance were investigated in this study.
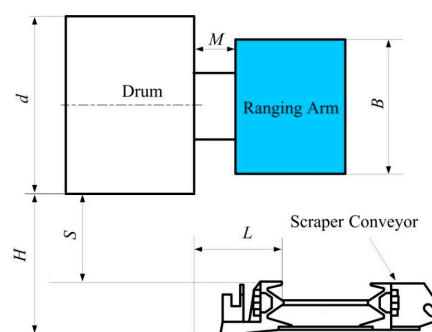

Figure 3. Drum position.

In China, the thin seam shearer used for mining primarily includes a front drum for ejection and a back drum for pushing. The drum and its simplified model are illustrated in Figure 4. Moreover,

the back drum has poor coal loading performance because the primary coal loading area is hindered by the ranging arm. The front drum is primarily responsible for the coal loading due to the poor coal loading performance of the back drum. Thus, the front drum was the primary objective in this study. Additionally, the effects of the drum position parameters and the thickness of the ranging arm on the coal loading performance were predicted. The scraper-based shearer could select from the following mining options: front drum to cut the roof, back drum to cut the bottom, front drum to cut the bottom, and back drum to cut the roof (Figure 2). However, the floor-based shearer could only use the front drum for cutting the bottom and the back drum for sweeping the roof. Hence, the value of S could be negative or positive. By analyzing the parameters of the thin seam shearer and the associated scraper conveyor equipment, which are made in China, the actual value of B is greater than 450 mm. The G value is within 200 mm, and the L value is greater than 250 mm. To compare with the test, the actual values of the simulation parameters were scaled down by a ratio of 1:2 based on the similarity theory. In our simulations, D_c, cutting depth, vane diameter, and drum hub diameter were 600, 530, 500 and 240 mm, respectively. The G value is 100 mm. The values of B were 275, 300, 325 and 350 mm. The values of S were -120, -60, 0, 60, 120 and 180 mm. The values of L were 150, 200, 250 and 300 mm. The height of the middle groove of the scraper conveyor is 120 mm. To achieve the desired simulation results and reduce the simulation time, the ranging arm was simplified to a combination of a closed cube and a closed cylinder, and the shovel board of the scraper conveyor and the ledge were replaced by tilting tetrahedrons. The particles that moved to the right of the tilting tetrahedrons were considered as loaded coal. A grey fixed wall of tilting tetrahedrons, which was parallel to the ground, was set between the scraper conveyor and the coal wall. A certain height had to be ensured to prevent particle accumulation at the scraper conveyor, which could worsen the conveying performance. The simulation model is illustrated in Figure 5, where the particle diameter is 30 mm, the particle friction factor is 0.8, the wall friction factor is 0.6, and the particle stiffness is 1×10^4 N·m. The statistical zone of the effective loaded particle is depicted in Figure 6, and the coal loading rate was calculated based on the statistical particle mass.
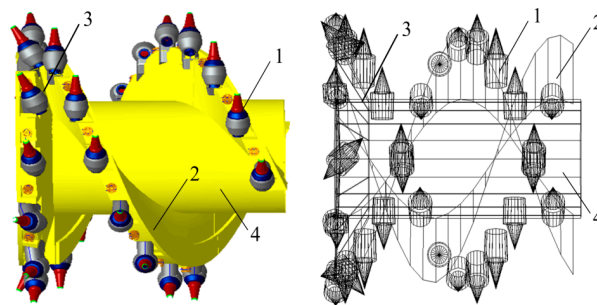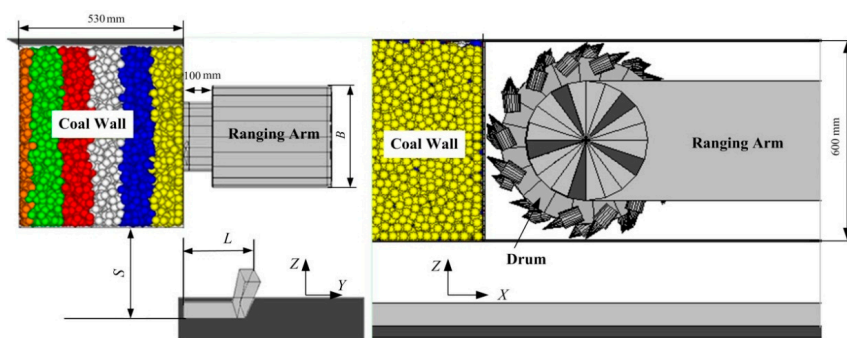

Figure 4. Drum and its simplified model.
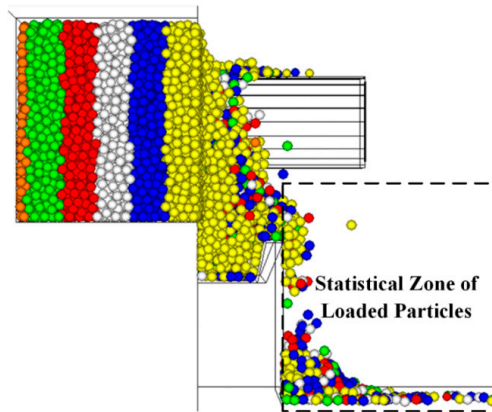

Figure 5. Simulation model of ranging arm.

Figure 6. Statistical zone of the effective loaded particle.

4. Results and Discussion

4.1. Effects of the Distance Between the Coal Wall and the Scraper Conveyor Middle Groove on the Drum Coal Loading Performance

To investigate the conveying performance influenced by the height of the drum bottom *S* in the middle groove of the scraper conveyor, the loading rate was simulated under different rotation speed and pulling speed combinations. The *S* values were −120, −60, 0, 60, 120 and 180 mm. In the simulations, *B* and *L* are 350 and 250 mm, respectively. Figure 7 demonstrates the simulation result when the speed is 2 m/min and the rotation speed is 60 r/min.

As indicated in Figure 7, the number of yellow and blue particles was the highest, white particles took second place, followed by red and green particles, and orange particles almost did not exist. It was illustrated that the closer the particles were to the inner position, the more difficult it was to be conveyed out. The accumulation surface was primarily composed of yellow particles, especially the space between the scraper conveyor and the coal wall. This is because the coal wall was cut from inside to outside by the pick, and the yellow particles were the closest to the shearer; thus, they were the last ones to be cut and conveyed in each rotation of the drum. Additionally, a few of the particles were ejected to the upside of the ranging arm, which was accorded with the practical results. Then, the effectiveness of the DEM was verified again. However, there were no significant differences in the number of loaded particles under the six different conditions (Figure 7). The key reason for this was that a few of the particles were conveyed to the statistical area whereas most of the particles were accumulated between the scraper conveyor and the coal wall. The simulation results for different *S* values were obtained in 18 seconds, and the statistical results are provided in Table 1.
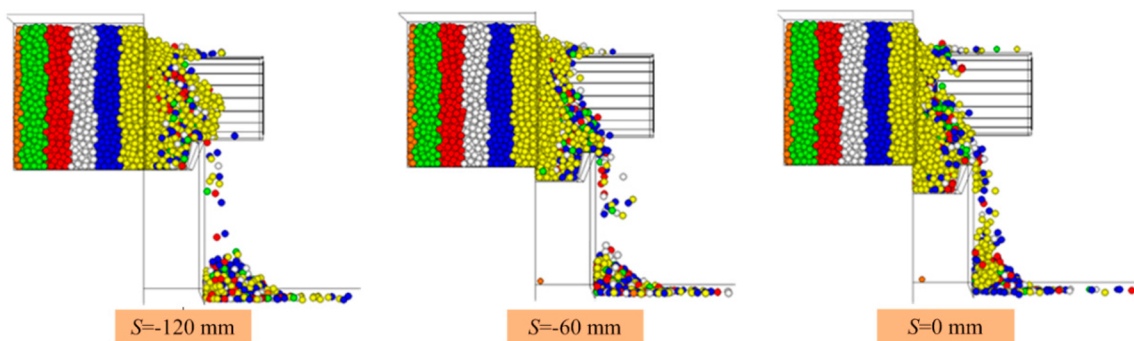

Figure 7. *Cont.*
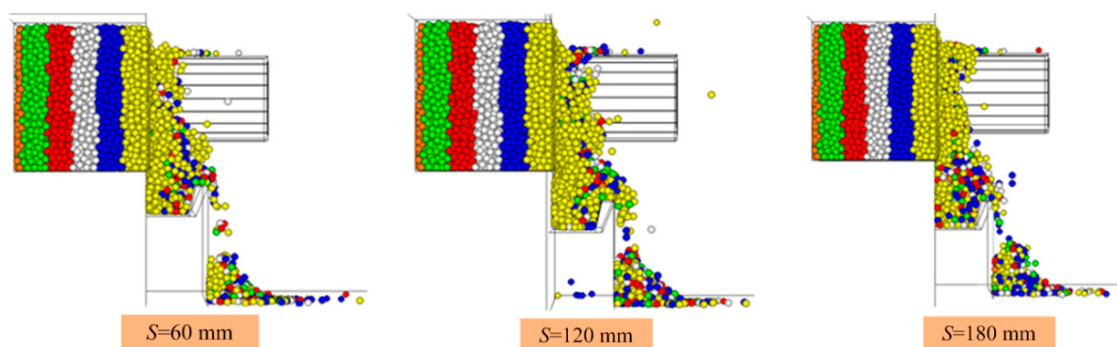
Figure 7. Simulation results for different *S* values.

Table 1. Simulation statistical results for different *S* values.

Hauling Speed (m/min)	Rotation Speed (r/min)	Vane Helix Angle (°)	*S* Value (mm)	Particle Accumulation Mass (kg)	Particle Loading Rate (%)
2	60	21	−120	14.34	23.73
2	60	21	−60	13.98	22.55
2	60	21	0	12.28	20.13
2	60	21	60	12.44	20.41
2	60	21	120	15.38	26.23
2	60	21	180	15.247	26.17
2	90	21	−120	14.97	24.45
2	90	21	−60	13.66	22.57
2	90	21	0	12.55	20.60
2	90	21	60	14.43	24.02
2	90	21	120	16.67	28.45
2	90	21	180	16.58	28.28
2	90	15	−120	13.35	22.00
2	90	15	−60	11.83	19.33
2	120	15	−120	17.55	29.01
2	120	15	−60	16.01	27.13
2	120	15	0	16.78	28.24
2	120	15	60	16.67	27.86
2	120	15	120	19.05	31.31
2	120	15	180	19.34	31.77

The loading rate first increased and then decreased with an increase in *S* (Figure 8 and Table 1). If *S* reached a certain value, the loading rate would remain constant. First, the *L* value was larger, and most of the coal particles could not load in the statistical area with the action of the drum. Then, they were accumulated in the region between the coal wall and the scraper conveyor, which was known as the *L* area in the study. When *S* was −120 mm, the motion traces of the ejection particles were impeded by the accumulated particles and remained in the *L* area. At that point, there were no obstacles on both sides of the *L* area, and the coal particles then accumulated naturally to a modest peak. Because of the gravitational attraction, the particles slid on both positions. A portion of them slid to the drum and moved again under the activity of the vane, and another part slid to the statistical area, thus improving the coal loading rate.

Subsequently, with an increase in the relative height of the drum, the blockade effect on the ejected particles was weakened. As the wall height on the left continually increased, the amount of particles needed to be increased to reach the accumulated balance in the *L* area. Within a certain wall height, the accumulated particles were intended to play a leading role, which reduced the amount of particles in the loading area and led to a decrease in the loading rate.

Lastly, the blockade effect on the ejected particles continued to decrease as the *S* value increased. Additionally, the accumulation angle gradually increased to a maximum, which illustrated that the number of accumulated particles had reached a stable state. Thus, the quantity of particles that

were loaded in the statistical area increased. The axial and tangential velocities of the particles after coming in contact with the vane depended on the drum rotation and the vane helix angle [27]. In the simulation, the vane helix angle and the drum rotation were 21° and 60 r/min, respectively, and the particles' axial velocity and tangential velocity were 18.16 m/min and 22.45 m/min, respectively. When the helix angle was 21° and the drum rotation was 90 r/min, the axial velocity and the tangential velocity of the particles were 27.2 and 33.76 m/min, respectively. When the helix angle decreased to 15° and the drum rotation increased to 120 r/min, the axial velocity and the tangential velocity of the particles were 29.5 and 29.47 m/min, respectively. When the axial velocity reached the above values, the particles were not directly loaded in the statistical area but in the *L* area, and they were even ejected from the top of the drum. The loading rate was essentially the same when *S* was 120 and 180 mm because the same number of particles was needed to balance the accumulation, which caused the same amount of particles to be loaded into the loading area.
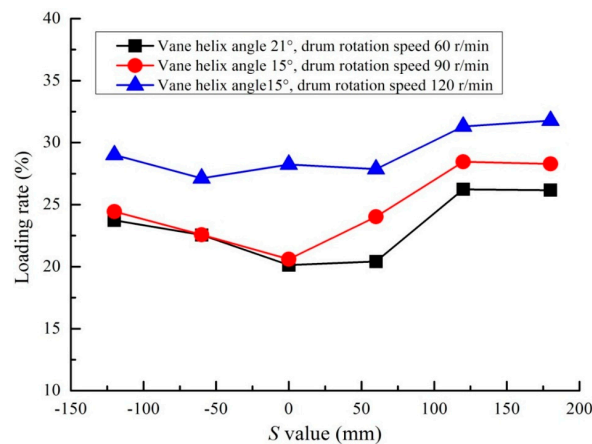

Figure 8. Variations in the particle mean loading rate for various *S* values.

As indicated in Figure 8, when the vane helix angle was 15° and the rotation speed was 120 r/min, the loading rate was greater than that when the vane helix angle was 21° and the rotation speed was 90 r/min. This is primarily because the cutting depth used in the simulation was less than the maximum theoretical value. Compared with the theoretical analysis, a smaller tangential velocity and a larger axial velocity were obtained in the DEM simulation.

Additionally, when $S \leqslant 0$ mm and the helix angle was 21°, the loading rate was essentially the same as when the rotation speed was 90 and 60 r/min. This result primarily occurred because the movement of the particle output was blocked by the accumulated particles in the *L* area. Moreover, the particles were ejected to both sides of the drum and accumulated behind the ranging arm. Furthermore, these particles were stopped due to the larger thickness and lower height of the ranging arm, thus they could not enter the *L* area, which resulted in the same loading rate as when $S \leqslant 0$ mm. However, when the *S* value continued to increase ($S \geqslant 0$), the loading rate was greater when the rotation speed was 90 r/min compared to when the rotation speed was 60 r/min. The distance between the bottom surface of the *L* area and the ranging arm increased with an increase in the height of the ranging arm, and this distance was larger than the height of the particles naturally accumulated on the rear of the drum. There was a length of 100 mm between the coal wall and the ranging arm, and a large number of particles, which belonged to the *L* area, entered this field. If the height of the accumulated particles in this area exceeded the natural accumulation height, then the particles would slide to the statistical areas; hence, the loading rate was greater when the rotation speed was 90 r/min compared to that of 60 r/min.

It can be understood from the above research that the loading rate would be smaller without considering the ranging arm and the distance *L*, when it exists. In the simulation, the loading rate reached a minimum value when the drum bottom had the same height as that of the middle groove

of the scraper conveyor. The coal loading was improved to a certain extent by increasing the *S* value or the drum rotation speed on the premise that the cutting depth was smaller than the theoretical upper limit value.

4.2. Effects of the Distance Between the Coal Wall and the Middle Groove of the Scraper Conveyor on the Drum Coal Loading Performance

Based on the above research, due to the accumulated coal in the *L* area after being outputted from the drum, the actual quantity of the coal loading decreased, and the following output performance was blocked, thus negatively impacting the coal loading performance. This result indicates that it is necessary to consider the influence of *L* on the coal loading rate in the design of the scraper conveyor and the drum. Thus, the influence of *L* on the coal loading rate was simulated and analyzed using the PFC^{3D} software. In the simulations, *S* = 60 mm and *B* = 350 mm, and the *L* values were 150, 200, 250 and 300 mm where the rotation speed was 60 r/min and the pulling speed was 2 m/min. The simulation results were obtained in 18 s.

In Figure 9, the loaded particles are mostly yellow, with a few white and red, which illustrated that the inner particles were hard to output, even if the distance between the coal wall and the middle groove of the scraper conveyor was varied. As seen from the accumulated particles figure, the surface of the *L* area is covered in yellow. With an increase in the *L* value, the amount of particles loaded in the statistical area clearly decreased. The simulation statistical results for different *L* values are provided in Table 2, and the time was 18 s.
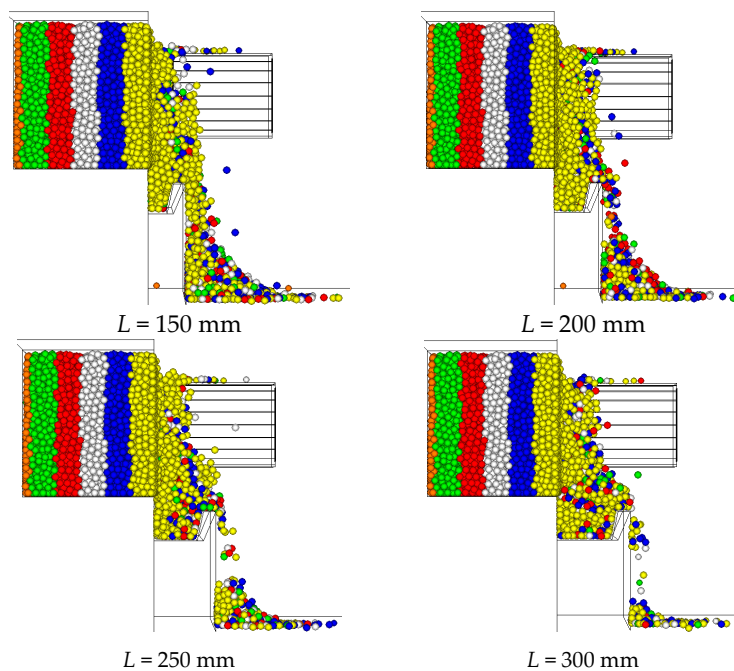

L = 150 mm	*L* = 200 mm
L = 250 mm	*L* = 300 mm

Figure 9. Simulation results for different *L* values.

Table 2. Simulation statistical results for different *L* values.

L Value (mm)	Particle Mean Velocity in *X*-Direction (m/s)	Particle Mean Velocity in *Y*-Direction (m/s)	Particle Mean Velocity in *Z*-Direction (m/s)	Particle Accumulated Mass (kg)	Particle Loading Rate (%)
150	0.0124	0.0102	0.0202	42.93	52.67
200	0.0121	0.0098	0.0139	26.71	38.61
250	0.0111	0.0082	0.0124	12.44	20.41
300	0.0114	0.0078	0.0096	4.32	7.54

The mean velocity in the *Y* and *Z* directions, the accumulated mass of the loaded particles, and the loading rate decreased with an increase in the *L* value (Table 2). The mean velocity in the *X* direction was less affected by the *L* value, and the trend was not obvious. The variation in the particle mean velocity in the *Y* direction and the particle loading rate for different *L* values can be analyzed based on Table 2, and the trend is illustrated in Figure 10. The particle loading rate decreased linearly with a decrease in the *L* value. The relationship between the average velocity in the *Y* direction and the *L* values had a similar trend; however, it was not an obvious linear trend compared with the relationship between the loading rate and the *L* values, which is because the particles should pass the *L* area first and then load in the statistical area. The movement in the *Y* direction was complex due to the existing *L* area. Compared with the loading rate for an *L* value of 150 and 300 mm, it was determined that the loading rate was significantly influenced by the distance between the coal wall and the middle groove of the scraper conveyor, and the loading rate reduced 3% for a 10 mm increase in the *L* value. Thus, the *L* value should be minimized in the design of the scraper conveyor and the shearer.
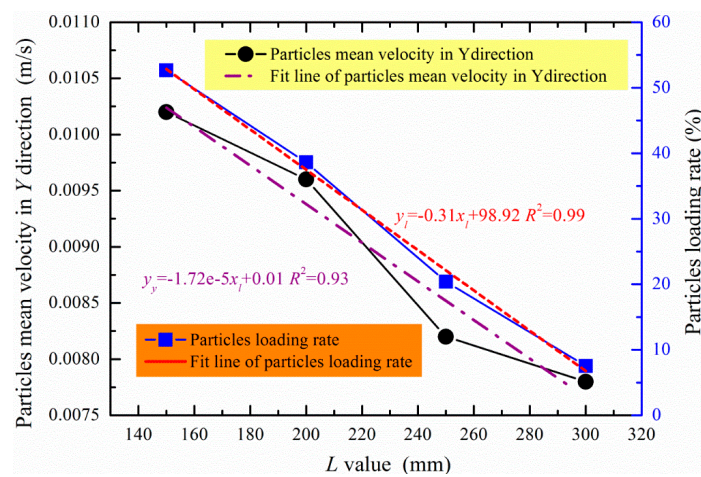

Figure 10. Variations in the particle's *Y* direction mean velocity and the particle loading rate for different *L* values.

4.3. Effects of the Thickness of the Ranging Arm on the Drum Coal Loading Performance

The particle outputs could be blocked by the ranging arm, and the particles were more likely to be blocked by a thicker ranging arm, which would cause a decrease in the loading rate. Thus, the particle output of the drum was studied using the established simulation model for different thicknesses of the ranging arm (275, 300, 325 and 350 mm) (Figure 11). In these simulations, *S* was 60 mm, and *L* was 260 mm. When the rotation speed was 60 r/min and the pulling speed was 2 m/min, the surface of the *L* area was primarily covered with yellow particles. When the thickness of the ranging arm B was 275 and 300 mm, red, green, blue and white particles appeared in the statistical area, and the red, green, and blue particles were evenly distributed. When *B* was 325 and 350 mm, the particles in the statistical area were primarily yellow, with a few other colors. This result indicated that the drum had a strong conveying capacity because the *B* was a smaller value. Furthermore, we determined that the mean velocity in the *Y* direction and the loading rate exhibited a general tendency to decrease with an increasing *B* value when the rotation speed was 60 r/min and the pulling speed was 2 m/min (Table 3). The mean velocity in the *X* and *Z* directions had no significant relationship with the thickness of the ranging arm. The variations in the particle *Y* direction mean velocity and the particle loading rate for different *B* values are provided in Figure 12. From the fitted curves, the mean velocity in the *Y* direction and the loading rate decreased as a quadratic function with an increase in the *B* value, but there was a large difference between them. This result occurred because the *L* value was greater in the simulation; thus, the particles could not be directly conveyed to the statistical area

and entered the *L* area first. Along with the different blockages of the ranging arm, the change in the mean velocity in the *Y* direction was complicated; however, it was similar to the trends of the loading rate.
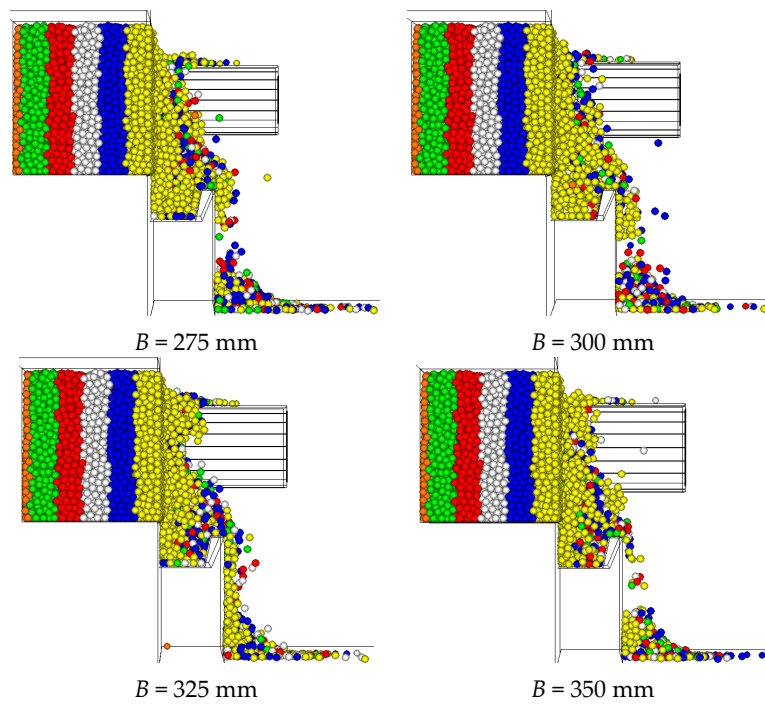

<div align="center">*B* = 275 mm   *B* = 300 mm</div>

<div align="center">*B* = 325 mm   *B* = 350 mm</div>

Figure 11. Simulation results for different *B* values.

Table 3. Simulation statistical results for different *B* values.

B Value (mm)	Particle Mean Velocity in *X*-Direction (m/s)	Particle Mean Velocity in *Y*-Direction (m/s)	Particle Mean Velocity in *Z*-Direction (m/s)	Particle Accumulated Mass (kg)	Particle Loading Rate (%)
275	0.0109	0.0088	0.0108	14.41	20.88
300	0.012	0.0086	0.0138	13.3	19.04
325	0.0122	0.0083	0.0108	10.95	18.78
350	0.0118	0.0082	0.0121	10.84	18.23

$y_b = 0.01 - 3.09\text{E-}5x + 3.6\text{E-}8x^2 \; R^2 = 0.93$

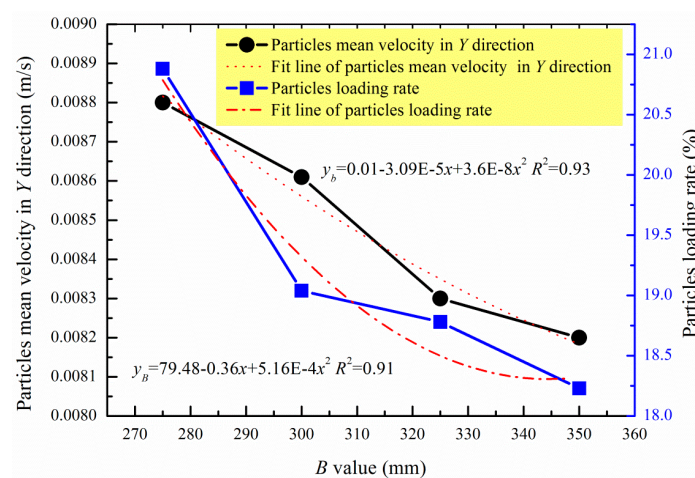$y_B = 79.48 - 0.36x + 5.16\text{E-}4x^2 \; R^2 = 0.91$

Figure 12. Variations in the particles' *Y* direction mean velocity and the particle loading rate for different *B* values.

In previous studies, for a greater drum rotation speed, the ejection effect of the vane on the particles was more evident. Additionally, in certain cases, for a higher position of the particles on the exit of the drum, the blockage became worse with an increase in the thickness of the ranging arm. To confirm this theory and study the influence of the thickness of the ranging arm on the loading rate for different rotation speeds, an additional study was conducted using the DEM. The results are provided in Table 4 and Figure 13, which illustrate that the loading rate decreased with an increase in the thickness of the ranging arm. As indicated in Figure 13, the rate of decrease of the loading rate was similar for 90 and 120 r/min, whereas the loading rate changed slightly for 60 r/min. If the rotation speed was slower, the particles would slide to the *L* area directly along the ranging arm due to the lower exit, smaller contact area with the ranging arm, and softer collision.

With the increase in the rotation speed, the exit velocity and the particle height increased as well as the blockage area of the ranging arm on the particles. Thus, the loading rate considerably decreased with the increase of the thickness of the ranging arm when the rotation speed was 90 and 120 r/min. Additionally, when the thickness of the ranging arm was small, the loading rate was higher for a rotation speed of 120 r/min than that for 60 r/min. With an increase in the thickness of the ranging arm, the resulting trend changes. In other words, the loading rate was lower for the 120 r/min rotation speed compared with the rotation speed of 60 r/min. Even when the rotation speed was 120 r/min, the amount of particle output was lower than it was for 60 r/min. A few of the particles could still pass the *L* area and load into the statistical area when the ranging arm was thinner, which was caused by the higher output speed. The loading rate clearly decreased with an increase in the thickness of the ranging arm because the blockage of the ranging arm became significant.

Table 4. Influence of the thickness of the ranging arm on the particle loading rate for different rotation speeds.

Hauling Speed (m/min)	Rotation Speed (r/min)	Vane Helix Angle (°)	*B* Value (mm)	Particle Accumulated Mass (kg)	Particle Loading Rate (%)
2	60	21	275	14.41	20.88
2	60	21	300	13.30	19.04
2	60	21	325	10.95	18.78
2	60	21	350	10.84	18.23
2	90	21	275	20.10	33.16
2	90	21	300	17.82	30.27
2	90	21	325	16.01	25.98
2	90	21	350	14.12	23.92
2	120	21	275	13.60	23.04
2	120	21	300	11.21	18.86
2	120	21	325	9.79	16.11
2	120	21	350	8.44	13.73
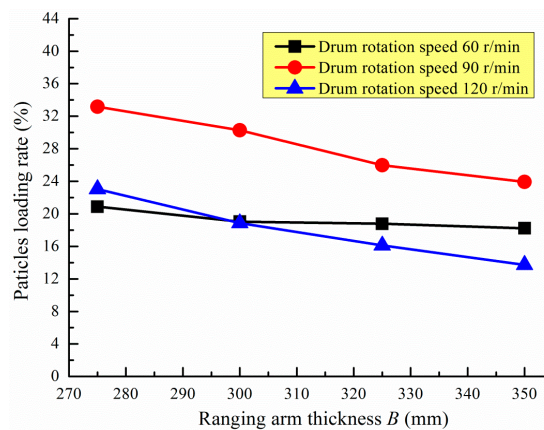
Figure 13. Variations in the particle loading rate with the thickness of the ranging arm B for different rotation speeds.

It can be concluded from the above analysis that the loading rate decreased with an increase in the thickness of the ranging arm within a small range when a lower rotation speed was used. Furthermore, the loading rate was significantly influenced by the thickness of the ranging arm when a higher rotation speed was used, especially when significant ejecting occurred. Thus, the thickness of the ranging arm should be reduced as much as possible in the design of the shearer.

5. Conclusions

Based on the structural characteristics and the working environment of thin coal seam shearers, the simulation model of an operational thin coal seam shearer ranging arm was established. The drum coal loading processes for different drum position parameters and different ranging arm thicknesses were simulated. Additionally, the effects of the related parameters on the coal loading performance of the shearer drum were obtained. The influence of the relative height between the drum and the scraper on the coal loading performance of the shearer drum was investigated. The results indicate that when the height of the drum bottom is consistent with the scraper, the drum coal loading performance is the worst; thus, the loading performance of the shearer drum can be increased by decreasing or increasing the drum height. An investigation on the effects of the distance between the coal wall and a scraper on the coal loading performance of the shearer drum was conducted. The results indicate that the distance is the most significant factor that affects the coal loading performance of the shearer drum, and the coal loading performance decreases linearly with an increase in the distance. Furthermore, our study indicates that the effects of the thickness of the ranging arm on the low-speed drum coal loading rate are not apparent, whereas the effects of the thickness of the ranging arm on the high-speed drum coal loading rate are evident. In summary, the current study provides a reference for improving the coal loading rate from the aspects of shearer structural design, mining technology selection, and scraper structural design.

Author Contributions: Kuidong Gao and Jianghui Dong conceived and designed the experiments, Kuidong Gao performed the experiments, Kuidong Gao, Qingliang Zeng and Changlong Du analyzed the data, and Kuidong Gao, Changlong Du and Jianghui Dong wrote the report.

Conflicts of Interest: The authors declare no conflict of interest.

References

1. Morris, C.J. The design of shearer drums with the aid of a computer. *The Min. Eng.* **1980**, *11*, 289–295.
2. Hurt, K.G.; Mcstravick, F.G. High performance shearer drum design. *Colliery Guard.* **1988**, *236*, 425–429.
3. Brooker, C.M. Theoretical and practical aspects of cutting and loading by shearer drums. *Colliery Guard.* **1979**, *1*, 9–16.
4. Ludlow, J.; Jankowski, R.A. Use lower shearer drum speed to achieve deeper coal cutting. *Min. Eng.* **1984**, *36*, 251–255.
5. Peng, S.S.; Chiang, H.S. *Longwall Mining*; John Wiley and Sons: New York, NY, USA, 1984.
6. Ayhan, M. Investigation into the Cutting and Loading Performance of Drum Shearers in OAL Mine. Master's Thesis, Institution of Science, The University of Hacettepe, Ankara, Turkey, 1994.
7. Ayhan, M.; Eyyuboglu, E.M. Comparison of globoid and cylindrical shearer drums' loading performance. *J. S. Afr. Inst. Min. Metall.* **2006**, *106*, 51–56.
8. Liu, Q.Y.; Yan, H.F. Symmetrical coefficient design of shearer drum. *J. China Univ. Min. Technol. Chin. Ed.* **1997**, *4*, 95–98.
9. Liu, S.Y.; Du, C.L.; Zhang, J.J.; Jiang, H. Parameters analysis of shearer drum loading performance. *Min. Sci. Technol.* **2011**, *5*, 621–624. [CrossRef]

10. Gao, K.D.; Du, C.L.; Liu, S.Y.; Fu, L. Model test of helical angle effect on coal loading performance of shear drum. *Int. J. Min. Sci. Technol.* **2012**, *22*, 165–168.

11. Gao, K.D.; Du, C.L.; Liu, S.Y.; Fu, L. Analysis on significance of the factors influencing shearer drum cutting performance. *Int. J. Oil Gas Coal Technol.* **2014**, *4*, 386–398. [CrossRef]

12. Shmulevich, I.; Asaf, Z.; Rubinstein, D. Interaction between soil and a wide cutting blade using the discrete element method. *Soil Tillage Res.* **2007**, *97*, 37–50. [CrossRef]

13. Ketterhagen, W.R.; Curtis, J.S.; Wassgren, C.R.; Kong, A.; Narayan, P.J.; Hancock, B.C. Granular segregation in discharging cylindrical hoppers: A discrete element and experimental study. *Chem. Eng. Sci.* **2007**, *22*, 6423–6439. [CrossRef]

14. Mukherjee, A.K.; Mishra, B.K. Experimental and simulation studies on the role of fluid velocity during particle separation in a liquid–solid fluidized bed. *Int. J. Miner. Process.* **2007**, *4*, 211–221. [CrossRef]

15. Labra, C.; Rojek, J.; Oñate, E.; Zarate, F. Advances in discrete element modeling of underground excavations. *Acta Geotech.* **2008**, *3*, 317–322. [CrossRef]

16. Nakashima, H.; Fujii, H.; Oida, A.; Momozu, M.; Kanamori, H.; Aoki, S.; Yokoyama, T.; Shimizu, H.; Miyasaka, J.; Ohdoi, K. Discrete element method analysis of single wheel performance for a small lunar rover on sloped terrain. *J. Terramech.* **2010**, *5*, 307–321. [CrossRef]

17. Su, O.; Akcin, N.A. Numerical simulation of rock cutting using the discrete element method. *Int. J. Rock Mech. Min.* **2011**, *3*, 434–442. [CrossRef]

18. Estay, D.A.; Chiang, L.E. Discrete crack model for simulating rock comminution processes with the Discrete Element Method. *Int. J. Rock Mech. Min.* **2013**, *60*, 125–133. [CrossRef]

19. McBride, W.; Cleary, P.W. An investigation and optimization of the 'OLDS' elevator using discrete element modeling. *Powder Technol.* **2009**, *3*, 216–234. [CrossRef]

20. Owen, P.J.; Cleary, P.W. Prediction of screw conveyor performance using the Discrete Element Method (DEM). *Powder Technol.* **2009**, *3*, 274–288. [CrossRef]

21. Osman, H.B. Granular Flow and Heat Transfer in a Screw Conveyor Heater: A Discrete Element Modeling Study. Ph.D. Thesis, National University of Singapore, Singapore, 2012.

22. Knuth, M.A.; Johnson, J.B.; Hopkins, M.A.; Sullivan, R.J.; Moore, J.M. Discrete element modeling of a mars exploration rover wheel in granular material. *J. Terramech.* **2012**, *1*, 27–36. [CrossRef]

23. Fu, L.; Du, C.L.; Li, J.P.; Gao, K.D. Discrete element simulation of the drill tool on the auger drill miner (DTAM) conveying coal. *Int. J. Earth Sci. Eng.* **2014**, *2*, 552–560.

24. PFC3D: User Manual. Itasca Consulting Group: Minneapolis, MN, USA, 2003.

25. Gao, K.D.; Du, C.L.; Fu, L.; Jiang, H.X. Effect of mining face angle on drum loading performance using discrete element method. *Int. J. Earth Sci. Eng.* **2014**, *1*, 41–51.

26. Gao, K.D. Feasibility of drum coal loading process simulation using three dimensional discrete element method. *Electron. J. Geotech. Eng.* **2015**, *14*, 5999–6007.

27. Roberts, A.W. The influence of granular vortex motion on the volumetric performance of enclosed screw conveyors. *Powder Technol.* **1999**, *1*, 56–67. [CrossRef]